Supplementary Information

Pathways to Pyrite: Direct Evidence for Metastable Precursors in Marine Sediments

Maria C Figueroa[1#*], Ravi K Kukkadapu[2#*], Daniel D Gregory[3], Anthony Chappaz[4], Mark H Engelhard[2], Timothy W Lyons[1]

[1]*Department of Earth and Planetary Sciences, University of California Riverside, Riverside, CA, 92521*

[2]*Environmental and Molecular Sciences Laboratory, Pacific Northwest National Laboratory, Richland WA, 99354*

[3]*Department of Earth Sciences, University of Toronto, 22 Ursula Franklin Street, Toronto, ON, M5S3B1*

[4]*STARLAB,* Earth and Atmospheric Sciences, Central Michigan University, Mount Pleasant, MI, 48859

[#] *co-first authors; *co-corresponding authors*

Table of Contents

Table S1. Modeled Mössbauer Spectral Parameters of 25 K and 10 K spectra

Sample	Phase[1]	<CS>[2] mm/s	<Δ>[3] mm/s	σ_D[4] mm/s	<ε>[5] mm/s	<|H|>[6] (T)	σ_{HFD}[7] (T)	phase %[8]	χ^2[9]
	Silicate Fe^{II}	1.28	2.87	0.17	—[10]	—	—	45.5	1.1
	Pyrite Fe^{II} (+minor silicate Fe^{III})	0.45	0.57	0.15	—	—	—	18.8	
S3 0-2 cm	Ilmenite	1	1	0.48	—	—	—	5	
(10 K)	np-FeS_{1+x}(*n*)	0.51	—	—	-0.02	27.9	4	20.5	
	np-FeS_{1+x} (*m*)	0.49	—	—	0.08	18.9	1	4.7	
	np-goethite (minor np-Mt)	0.4	—	—	0.04	51.1	2.5	5.6	
	Silicate Fe^{II}	1.28	2.89	0.17	—	—	—	40	0.9
	Pyrite Fe^{II} (+minor silicate Fe^{III})	0.45	0.6	0.15	—	—	—	22.7	
S3 40-42 cm	Ilmenite	1	1	0.48	—	—	—	5.1	
(25 K)	np-FeS_{1+x}(*n*)	0.62	—	—	0.01	28.2	4	21.2	
	np-FeS_{1+x}(*m*)	0.58	—	—	0.05	20.4	1	4.8	
	np-goethite (minor np-Mt)	0.4	—	—	0.04	51	2.5	6.2	
	Silicate Fe^{II}	1.28	2.86	0.17	—	—	—	41.4	1.1
	Pyrite Fe^{II} (+minor silicate Fe^{III})	0.45	0.57	0.15	—	—	—	21.9	
S4 0-2 cm	Ilmenite	1	1	0.48	—	—	—	5.9	
(10 K)	np-FeS_{1+x}(*n*)	0.36	—	—	-0.02	29.9	3	12.2	
	np-FeS_{1+x}(*m*)	0.28	—	—	-0.22	20.6	1	6.5	
	np-goethite (minor np-Mt)	0.6	—	—	-0.22	50.5	2.5	12.1	
	Silicate Fe^{II}	1.28	2.88	0.17	—	—	—	44.2	1.3
	Pyrite Fe^{II} (+minor silicate Fe^{III})	0.43	0.63	0.14	—	—	—	24.8	
S4 26-28 cm	Ilmenite	1	1	0.48	—	—	—	7.6	
(10 K)	np-FeS_{1+x}(*n*)	0.64	—	—	-0.44	29.9	5	9.9	
	np-FeS_{1+x}(*m*)	0.54	—	—	-0.14	18.2	2	7	
	np-goethite (minor np-Mt)	0.54	—	—	-0.16	50.5	3.5	6.5	

[1]Spectral component; [2]center shift; [3]quadrupole splitting; [4]std dev of Δ; [5]quadrupole shift parameter; [6]absolute average HF; [7]std deviation of hyperfine field distribution (HFD); [8]based on a fit on a sample and standard deviation; [9]goodness of fit; [10]not applicable. Np-Mt is nanoparticulate magnetite.

Lorentzian half widths at half maximum (HWHM) of all elemental doublets/sextets is fixed at 0.156 mm/sec; No coupling was allowed between CS and D ; the A+/A- areas of doublet are fixed at 1. No coupling is allowed between D and HF, and A1/A3 and A2/A3 are fixed at 3 and 2, respectively.
Modeling: Voight-based structural fitting routine (Rancourt and Ping, 1991).

Spectra for top and bottom layers from the basin sediments (S3)

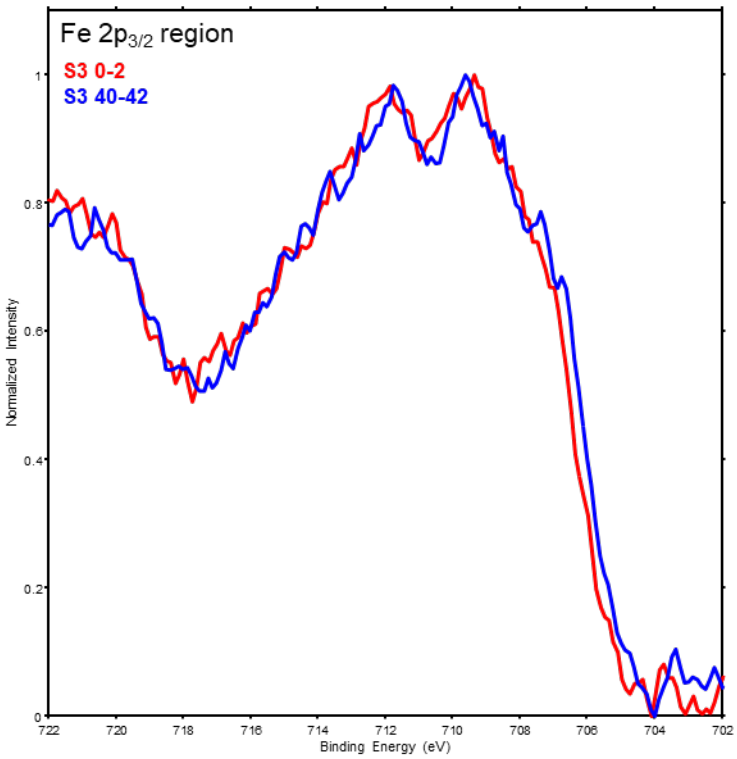

Figure S1. X-ray photoelectron spectroscopy (XPS) Fe2p spectra of the surface (0-2 cm; red) and deeper (40-42 cm; blue) sediment layers from the basin site (S3). The spectra exhibit similar peak positions and relative intensities, indicating consistent Fe speciation across both depths and comparable Fe mineralogy between the two layers.

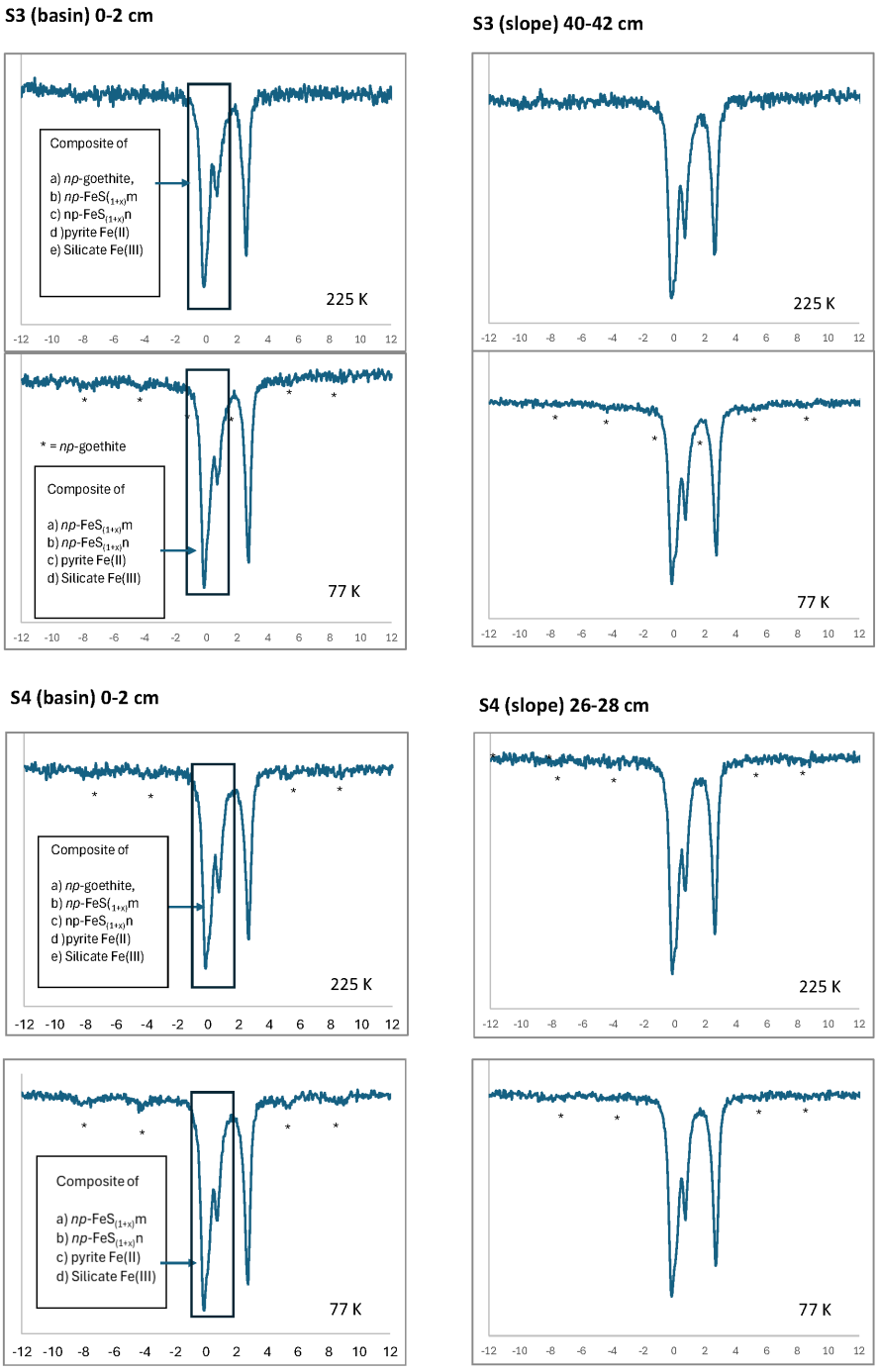

Figure S2. Mössbauer spectra showing np-goethite and np-FeS_{1+x} determination at 225 K and 77 K. The distinct sextet features characteristic of crystalline goethite are absent in all the sediment samples at 225 K. In contrast, the sextet features consistent with laboratory synthesized superparamagnetic nanoparticulate (np)-goethite[1] (denoted by * in the spectra) are visible at 77 K for all the samples. The Fe^{III}-(oxyhydr)oxide sextet at 77 K (qualitative fits) and those of the 10 K spectra appear similar, but the presence of superparamagnetic FeS_x species hinders the unique fits at 77 K. This similarity unambiguously indicates the absence of ferrihydrite in these samples, as ferrihydrite and goethite exhibit nearly identical MBS parameters at near 4.2 K, unlike at 77 K[2]

Typical FeS_x sextet features evident in the 77 K laboratory-synthesized model compounds[3] are absent in our sediments. Nonetheless, there's a strong correlation between our 10 K and 25 K FeS_x spectral features and the FeS_x 5 K spectra from the study of Schroder et al. (2020). This comparison suggests that FeS_x in our sediments is smaller than in the synthetic compounds. These discrepancies lead us to classify our FeS_x compounds as np-$FeS_{(1+x)}$(n) and np-$FeS_{(1+x)}$(m), respectively. We also generated 5 K spectra to establish parallels with synthetic FeS_x 5 K spectra from the study of Schroder et al. (2020); however, extensive clay Fe^{II} magnetic ordering at this temperature prevented suitable correlations with the laboratory-synthesized FeS_x samples.

Table S2. Sequential Fe extraction results comparing two approaches for calculating highly reactive iron (Fe_{HR}).

	Fe_{py} (Fe_{CRS} + Fe_{AVS})	Fe_T	Fe_T/Al	Fe_{HR} + (Fe_{ace} + Fe_{ox})	Fe_{HR} - (Fe_{ace} + Fe_{ox})	Fe_{HR}/Fe_T	Fe_{py}/Fe_{HR}
S3 0-2	1.03	5.19	0.55	1.80		0.35	0.57
					1.45	0.28	0.70
S3 40-42	0.88	3.91	0.57	1.86		0.48	0.48
					1.36	0.35	0.65
S4 0-2	0.66	4.15	0.51	1.28		0.31	0.52
					0.94	0.23	0.70
S4 26-28	0.78	4.19	0.47	1.28		0.30	0.61
					1.00	0.24	0.78

Values are given in weight percentage (wt%) for pyrite Fe (Fe_{py}) and total Fe (Fe_T). Fe_{HR} are calculated both including (grey shade) and excluding (black shade) carbonate (Fe_{ace}) and magnetite (Fe_{ox}) associated fractions.

The Fe_{HR} proxy was originally defined as the sum of pyrite and Fe-oxides ($Fe_{HR} = Fe_{py} + Fe_{ox}$) to distinguish anoxic from oxic conditions (Raiswell & Canfield, 1998). A later calibration extended this definition to include Fe-carbonates and magnetite ($Fe_{HR} = Fe_{py} + Fe_{ox} + Fe_{carb} + Fe_{mag}$) in some modern sediments (Poulton & Canfield, 2005). However, Raiswell et al. (2018) emphasized that this extended calculation should only be applied when Fe-carbonates and magnetite are demonstrably present and reactive to porewater sulfide on early-diagenetic timescales. In our modern Saanich Inlet sediments, Fe_{HR} fractions include Fe from CRS (pyrite), AVS, Fe_{asc} (ferrihydrite and amorphous oxides), and Fe_{dith} (crystalline oxides), plus/minus Fe_{ace} (Fe-carbonates, siderite) and Fe_{ox} (magnetite). Mössbauer spectroscopy, however, confirmed that neither Fe-carbonates nor crystalline magnetite are present, indicating that fractions attributed to these phases in the extractions should not be included in Fe_{HR}. Indeed, using the extended calculation misclassifies our S3 samples as ferruginous, while the original definition correctly classifies all samples as fluctuating redox with high sedimentation (Fig. S3). FeT/Al ratios (0.47–0.57) fall within the detrital baseline for modern sediments (0.55 ± 0.11), indicating no water-column Fe enrichment and further supporting exclusion of carbonate and magnetite. Using the original Fe_{HR} definition,

Fe_{HR}/Fe_T values indicate low oxygen, while Fe_{py}/Fe_{HR} ratios of 0.70–0.78 point to sulfidic porewaters. The slightly lower ratio (0.65) in the deeper basin sediment reflects methanic conditions that limits pyrite formation. Together, these results confirm that the Fe proxy remains robust for paleoredox reconstructions, provided that Fe_{HR} is calculated according to mineralogical context and the criteria outlined by Raiswell et al. (2018).

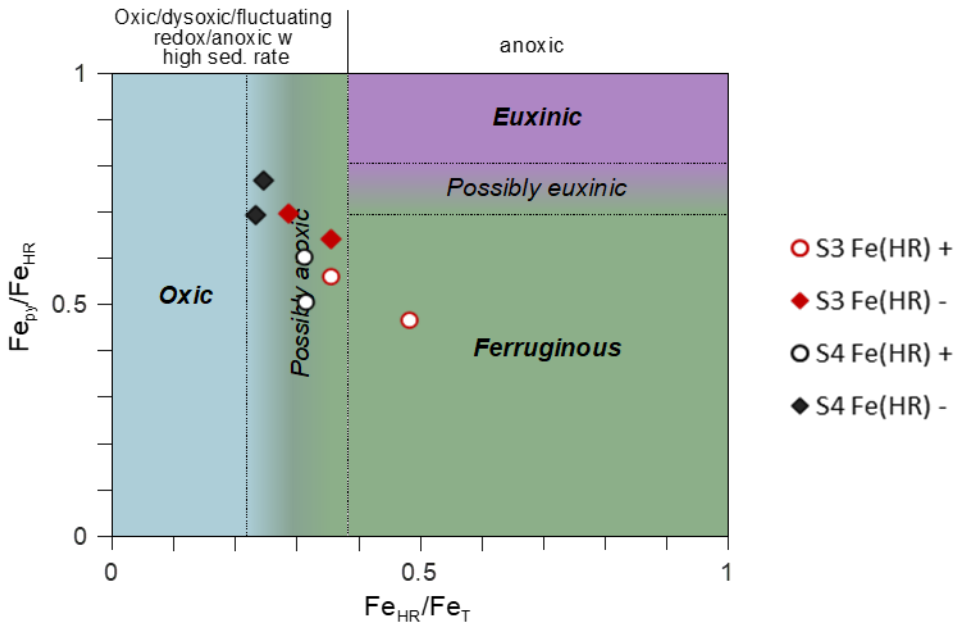

Figure S3. Comparison of Fe speciation results from Saanich Inlet sediments plotted within the framework of paleoredox fields defined by Fe_{HR}/Fe_T versus Fe_{py}/Fe_{HR} (after Poulton & Canfield, 2011). Symbols distinguish values calculated using the inclusive definition of Fe_{HR} (Fe_{HR} + [Fe_{ace} + Fe_{ox}], circles) versus the exclusive definition (Fe_{HR} – [Fe_{ace} + Fe_{ox}], diamonds). Basin samples (S3, red) and slope samples (S4, black) are shown. The placement of data points illustrates how different Fe_{HR} definitions influence classification within oxic, ferruginous, and euxinic fields.